Mechanisms of two-color laser-induced field-free molecular orientation

Michael Spanner,[1] Serguei Patchkovskii,[1] Eugene Frumker,[2,3,4] and Paul Corkum[2]

[1] *Steacie Institute for Molecular Sciences, National Research Council of Canada, Ottawa, ON, Canada K1A 0R6*
[2] *Joint Attosecond Science Laboratory, University of Ottawa and National Research Council of Canada, 100 Sussex Drive, Ottawa, On, Canada*
[3] *Department of Physics, Texas A&M University, College Station, Texas 77843, USA*
[4] *Max-Planck-Institut für Quantenoptik, Hans-Kopfermann-Strasse 1, D-85748 Garching, Germany*

(Dated: August 7, 2018)

Two mechanisms of two-color ($\omega + 2\omega$) laser-induced field-free molecular orientation, based on the hyperpolarizability and ionization depletion, are explored and compared. The CO molecule is used as a computational example. While the hyperpolarizability mechanism generates small amounts of orientation at intensities below the ionization threshold, ionization depletion quickly becomes the dominant mechanism as soon as ionizing intensities are reached. Only the ionization mechanism leads to substantial orientation (e.g. on the order of $\langle\cos\theta\rangle \gtrsim 0.1$). For intensities typical of laser-induced molecular alignment and orientation experiments, the two mechanism lead to robust, characteristic timings of the field-free orientation wave-packet revivals relative to the the alignment revivals and the revival time. The revival timings can be used to detect the active orientation mechanism experimentally.

Laser-induced field-free alignment of small gas phase molecules, where the molecular axis is aligned along particular direction (see Fig.1), is now routine [1] and is a quickly becoming a central tool to in attosecond [2] and photoionization [3] experiments. Much less studied is the laser-induced field-free orientation of polar molecules, where both the molecular axis and the asymmetry point along a particular direction, which has recently been achieved [4] using two-color ultrafast pulses built from a fundamental and its second harmonic. The underlying physical effect thought to be responsible for the orientation is the hyperpolarizability interaction [4, 5]. However, it is possible that a second mechanism – ionization depletion – is operative, where a two-color ultrafast pulse selectively ionizes molecules at particular angles with respect to the polarization direction of the laser field. Hyperpolarizability generates orientation by causing an asymmetrical force that pushes the molecules toward orientation, while ionization depletion generates orientation by directly carving out an asymmetrical angular distribution upon ionization. In this work we implement a simple model of the ionization depletion mechanism, and contrast and compare the two mechanisms. A rigid linear rotor is used as an example system. Extension to symmetric and asymmetric tops is conceptually straightforward. Rotor parameters corresponding to the CO molecule are used in numerical examples.

The two-color laser pulse is written as

$$E(t) = E_0 f(t)[\cos(\omega t) + \cos(2\omega t)], \tag{1}$$

where $f(t)$ is the pulse envelope ($0 \le f(t) \le 1$), and E_0 (a positive real number) controls the peak electric field strength. The relative phase of the two fields was set to zero, and their relative amplitudes were set to one, in order to maximize the field asymmetry that leads to orientation. The nuclear rotation effectively does not respond on the timescale of the carrier oscillations, and it is then appropriate to use the cycle-averaged rotational Hamiltonian of the system:

$$H(\theta, t) = BJ(J+1) + V_P(\theta, t) + V_H(\theta, t) + V_I(\theta, t), \tag{2}$$

where B is the rotational constant, $V_P(\theta, t)$ is the polarizability term that generates molecular alignment [6], $V_H(\theta, t)$ is the hyperpolarizability term, and $V_I(\theta, t)$ accounts for ionization (see below). All equations use Hartree atomic units ($m_e = e = \hbar = 1$). For $E(t)$ in Eq. 1, the two middle terms in Eq. 2 are given by [5]

$$V_P(\theta, t) = -\frac{1}{2}\Delta\alpha E_0^2 |f(t)|^2 \cos^2\theta \tag{3}$$

$$\begin{aligned} V_H(\theta, t) \;=\; & -\frac{3}{8}\beta_{xxz} E_0^3 |f(t)|^3 \cos\theta \\ & -\frac{1}{8}(\beta_{zzz} - 3\beta_{xxz}) E_0^3 |f(t)|^3 \cos^3\theta \end{aligned} \tag{4}$$

where $\Delta\alpha = \alpha_\parallel - \alpha_\perp$ is the polarizability anisotropy, and the β_{ijk} are elements of the hyperpolarizability tensor. The molecular constants chosen to model CO are given in Table I.

Ionization is introduced using a complex absorbing potential

$$V_I(\theta, t) = -(i/2)\Gamma_I(\theta, t) \tag{5}$$

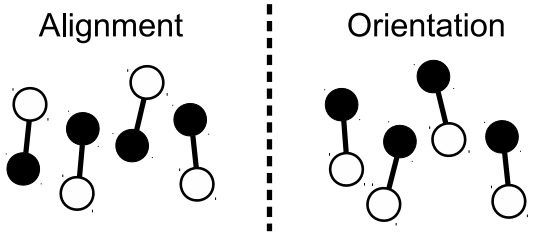

FIG. 1: Cartoon illustrating the difference between alignment and orientation of a schematic polar diatomic molecule.

TABLE I: Molecular constants (a.u.) used to model CO.

Parameter	Value [Ref.]	Parameter	Value [Ref.]
B	8.7997×10^{-6} [7]	$\Delta\alpha$	3.6 [8]
β_{zzz}	28.91 [8]	β_{xxz}	7.69 [8]
I_p	0.516 [7]	c_0	0.2214×10^{-3}
c_1	-0.2141×10^{-3}	c_2	0.0822×10^{-3}

where $\Gamma_I(\theta,t)$ is the cycle-averaged ionization rate. The remaining time-dependence of $\Gamma_I(\theta,t)$ arises from the pulse envelope $f(t)$. The complex potential causes non-unitary quantum evolution that removes amplitude as a function of angle, modeling the effects of population loss due to ionization. For simplicity, a separable form of $\Gamma_I(\theta,t)$ is assumed

$$V_I(\theta,t) = -(i/2)K(t)\Gamma_{\rm ref}(\theta), \tag{6}$$

where $\Gamma_{\rm ref}(\theta)$ is the cycle-averaged angular ionization rate calculated at a characteristic field strength $E_{\rm ref}$, and

$$K(t) = \exp\left(-\frac{2}{3}(2I_p)^{3/2}\left[|E_0 f(t)|^{-1} - |E_{\rm ref}|^{-1}\right]\right) \tag{7}$$

is the tunneling exponent [9, 10] that provides the dominant scaling of strong field ionization. I_p in Eq. 6 is the ionization potential of the molecule. Scaling in Eq. 6 qualitatively captures the ionization yield in small molecules over several orders of magnitude in laser intensity [11].

Calculation of $\Gamma_{\rm ref}(\theta)$ for ionization of $X^1\Sigma^+$ CO to $X^2\Sigma^+$ CO^+ is carried out using the time-dependent mixed orbital/grid method of Ref. [12], in the single-channel approximation. The wavefunctions of the neutral

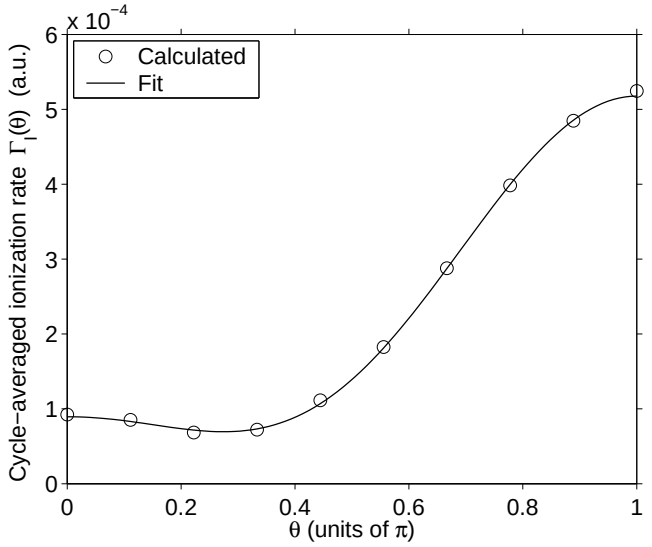

FIG. 2: Cycle-averaged ionization rate $\Gamma_{\rm ref}(\theta)$ Shown are the numerically calculated rates, and the fit from Eq. (8).

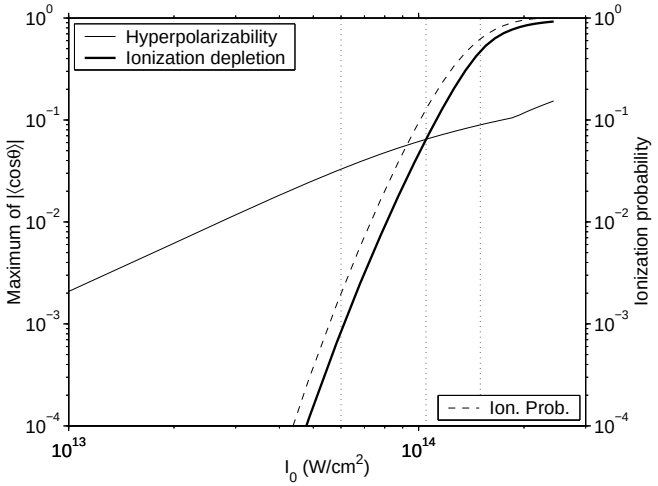

FIG. 3: Left axis: the maximum field-free orientation ($|\langle\cos\theta\rangle|$) after application of the two-color pump, as a function of pump intensity. Each of the two colors in the pump pulse has intensity I_0. Thin line: the hyperpolarizability mechanism. Thick line: ionization depletion. Right axis: total ionization probability (dashed line). The vertical dotted lines gives the intensities used in Figs. 4 and 5

and the ion are calculated using GAMESS-US [13] with the cc-pVTZ basis set [14] at the complete active space level using 10/9 (neutral/cation) active electrons in 8 orbitals. Uniform Cartesian grid extended to ±13 Bohr, with spacing of 0.2 Bohr. The time step was 0.002666 a.u. The simulation was run for a full cycle of the two-color field Eq. (1), with $E_0 = E_0^* = 0.0535$ ($I_0 = 10^{14}$ W/cm^2), $\omega = 0.057$ (λ =800/400 nm) followed by 2 fs at zero field. The cycle-averaged ionization rate was calculated by integrating the flux absorbed [15] at the edges of the grid, and dividing by the cycle duration ($2\pi/\omega$). Fig. 2 plots the calculated $\Gamma_{\rm ref}(\theta)$. Also shown is the fit given by a truncated Fourier series (see Table I):

$$\Gamma_{\rm ref}(\theta) = c_0 + c_1\cos\theta + c_2\cos 2\theta \tag{8}$$

All subsequent calculations use the fit of Eq. 8 in Eq. 6.

Although the Hamiltonian (2) includes both the hyperpolarizability and ionization terms, numerical results below consider the two mechanisms individually, to elucidate the characteristic features in the induced orientation. Simulations with both mechanisms active simultaneously did not reveal any qualitatively new features, and will not be discussed.

The initial populations of rotational states $|J,M\rangle$ are given by the Boltzmann distribution at temperature $T =$ 50K:

$$P(J,M) = \frac{\exp(-BJ(J+1)/kT)}{\sum_{J'}(2J'+1)\exp(-BJ'(J'+1)/kT)} \tag{9}$$

The time evolution of each rotational state within the ensemble is expanded in a spherical harmonics basis

$$|\Psi(t)\rangle = \sum_J a_J(t)|J,M\rangle. \tag{10}$$

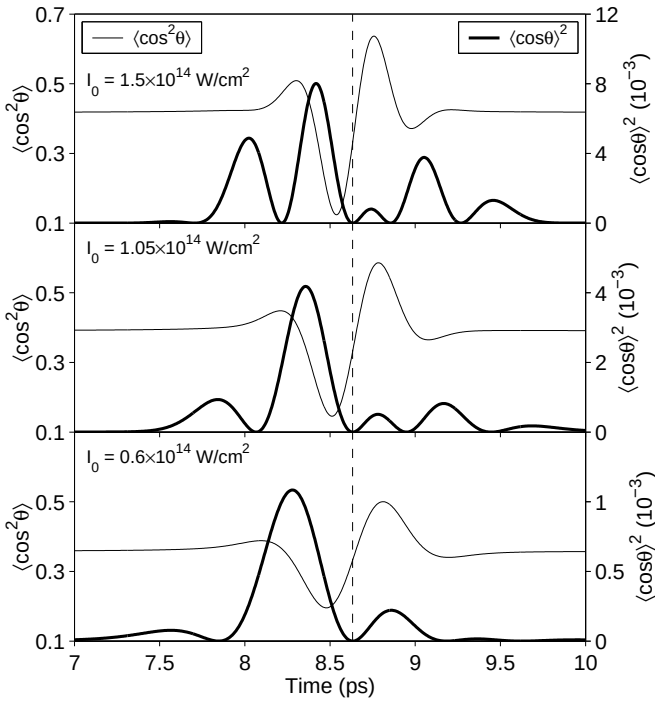

FIG. 4: The hyperpolarizability orientation mechanism. Alignment (thin line, left axis) and orientation (thick line, right axis) wave-packet revivals for a selection of intensities. The vertical dashed line denotes the revival time t_{rev}.

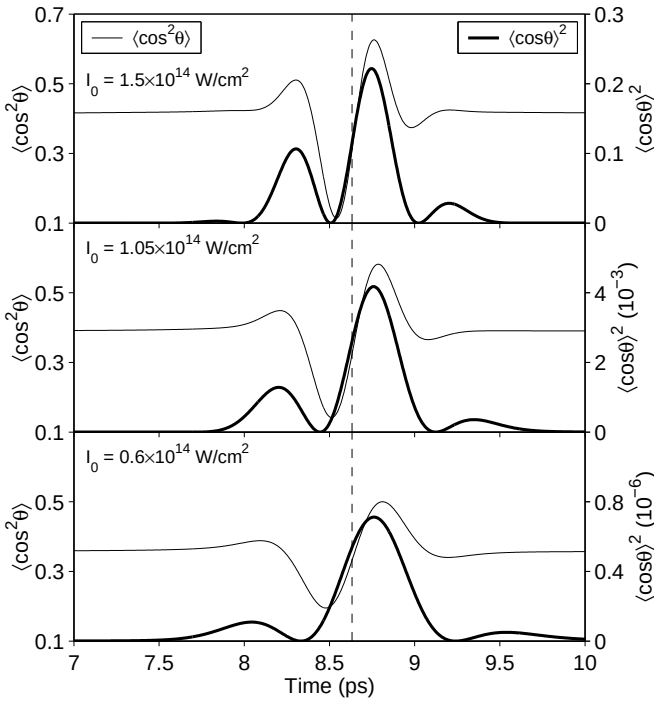

FIG. 5: The ionization depletion mechanism. See Fig. 4.

The single sum over J is appropriate since the Hamiltonian in Eq. (2) conserves M. The Schrödinger equation for the coefficients $a_J(t)$ is

$$i\frac{\partial}{\partial t}a_J(t) = BJ(J+1)a_J(t) + \sum_{J'}\langle J,M|V_P+V_H+V_I|J',M\rangle a_{J'}(t). \quad (11)$$

The envelope function $f(t)$ is defined as

$$f(t) = \begin{cases} 0, & t<0 \\ \sin(\pi t/2\tau_{on}), & 0<t<2\tau_{on} \\ 0, & t>2\tau_{on} \end{cases} \quad (12)$$

corresponding to a $\sin^2$ pulse for the intensity $I = E^2$. The parameter τ_{on} ($\tau_{on} = 30$ fs) is the full width at half-intensity. While the pulse is on ($t \le 2\tau_{on}$), Eq. (11) is solved using the Crank-Nicholson method [16]. After the end of the pulse ($t > 2\tau_{on}$), the analytical field-free propagation solution is used. Each initial $|J,M\rangle$ state is propagated independently. The observables are averaged over the thermal distribution $P(J,M)$.

The maximum field-free orientation following the pulse is shown in Figure 3, as a function of the single-color intensity $I_0 = E_0^2$. The orientation is characterized using the observable $\langle\cos\theta\rangle$. The total ionization probability is also shown (dashed line, right axis) on the same figure. The peak orientation scales very differently with the intensity for the two mechanisms. The hyperpolarizability mechanism shows the expected $I_0^{3/2}$ scaling. The depletion mechanism shows the same scaling as the ionization probability, coming from the tunneling exponent (Eq. 7).

At low intensities, where ionization is not possible hyperpolarizability provides the dominant mechanism of orientation generation. When the intensity increases and substantial ionization occurs, ionization depletion dominates the orientation. For the present model, the cross-over occurs at 1.05×10^{14} W/cm^2. This cross-over intensity is sensitive to the exact molecular parameters used, especially to the ionization rate model. Although qualitatively reasonable, Eqs. (6)-(8) are not expected to be quantitatively accurate, and consequently gives only a rough estimate of the experimental cross-over intensity. Due to the rapid increase in the peak orientation once ionization is active, it is likely that ionization depletion will be the active mechanism when the largest degrees of orientation are reached, regardless of the intensity where the mechanisms switch. Further, since the peak orientation for the ionization mechanism parallels closely the ionization probability, it follows that substantial orientation requires substantial ionization. For example, reaching an orientation of $\langle\cos\theta\rangle \gtrsim 0.1$ requires ionizing more than 10% of the sample in the CO case.

During short-pulse alignment and orientation, the molecular ensemble undergoes wave-packet revival dynamics, where short periods of sharp angular localization leading to strong alignment and orientation (the wave-packet revivals) are separated by longer periods charac-

terized by dispersed wavefunctions. Figures 4 and 5 show the alignment and orientation revivals at the first full revival $t_{rev} = \pi/B \approx 8.64$ ps. The alignment is characterized by the commonly-used alignment parameter $\langle\cos^2\theta\rangle$. The orientation is tracked using $\langle\cos\theta\rangle^2$, the square of the directional orientation parameter $\langle\cos\theta\rangle$. Note that $\langle\cos\theta\rangle^2$ does not contain the orientation direction. This is the appropriate observable to characterize some experimental orientation probes, such as high-harmonic generation [17]. For the present study, this observable conveniently draws out the peak orientation independent of direction.

At all intensities, the hyperpolarizability mechanism leads to peak orientation at early times relative to t_{rev} (Fig. 4). Since t_{rev} is also typically near the center of the alignment revival, the shift of the orientation wavepacket relative to t_{rev} can also be seen as a shift toward, and beyond, the minimum of the alignment revival. Ionization depletion, on the other hand, leads to the peak orientation shifted to later times relative to t_{rev} and to the alignment revival (Fig. 5). Thus, the relative timing between the peak of orientation and the alignment revival can be used to determine the active mechanism of orientation experimentally.

It is instructive to examine the origin of the relative timings within the two orientation mechanisms analytically, using the impulsive approximation. If the pulse duration is much shorter than typical rotation timescales ($\tau_{on} \ll 1/B$), the Hamiltonian of Eq. 2 becomes

$$H = BJ(J+1) + [V_P'(\theta) + V_H'(\theta) + V_I'(\theta)]\,\delta(t). \quad (13)$$

where $V_i'(\theta) = \int V_i(\theta,t)dt$. Without sacrificing any of the essential physics of the model, the potentials V_i' can be approximated by the leading non-constant terms in the $\cos\theta$ expansion

$$V_P'(\theta) \approx -\lambda_P \cos^2\theta \quad (14a)$$
$$V_H'(\theta) \approx -\lambda_H \cos\theta \quad (14b)$$
$$V_I'(\theta) \approx -i\lambda_I \cos\theta. \quad (14c)$$

where the numerical parameters (at the single-color intensity $I_0 = 6.0\times10^{13}$ W/cm^2) are $\lambda_P = 3.823$, $\lambda_H = 0.2561$, and $\lambda_I = 1.095\times10^{-3}$. The $t = +0$ wavefunction then becomes [18]

$$|\Psi\rangle = \exp\left[i\lambda_P\cos^2\theta + (i\lambda_H - \lambda_I)\cos\theta\right]|\Psi_0\rangle. \quad (15)$$

Impulsive orientation revivals for $I_0 = 6.0\times10^{13}$ W/cm^2 and the initial ensemble temperature of 50K are shown in Fig. 6. The impulsive approximation reproduces the temporal structure of the revivals seen in the full simulations (cf. the bottom panel of Fig. 6 to the bottom panels of Figs. 4 and 5). Thus, the temporal signature of the orientation is unrelated to the finite pulse duration effects. Furthermore, the orientation revival timings are not affected by the fine details of the angular dependence of the field-molecule interaction, and are robust.

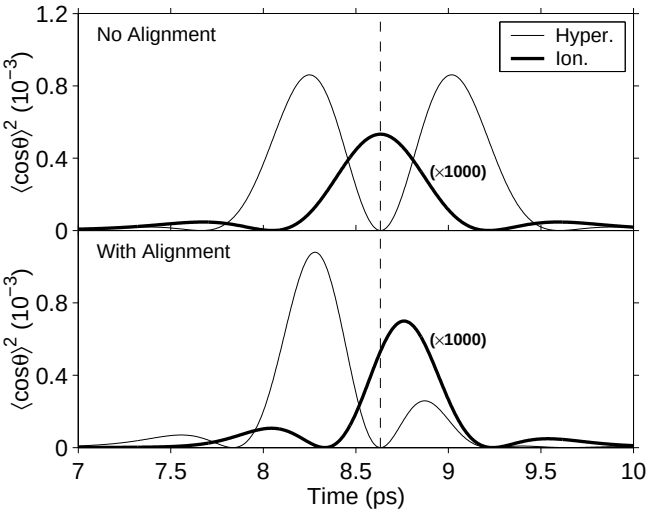

FIG. 6: Orientation revivals within the impulsive approximation ($I_0 = 6.0\times10^{13}$ W/cm^2). The ionization depletion results are scaled by a factor of 1000. Top panel: revival structure with the alignment interaction turned off ($\lambda_P = 0$). Bottom panel: with the alignment interaction included. The vertical dashed line denotes the revival time t_{rev}.

Consider now the orientation generated with alignment interaction turned off (Fig. 6, top). Both mechanisms generate revivals that are completely symmetric around t_{rev}. The hyperpolarizability revivals have a zero at t_{rev} and peak a short time after. The ionization depletion generates an orientation peak exactly at t_{rev}. The alignment-free behavior of the orientation is easy to understand. The rotational wavepacket is periodic, with period of t_{rev}. Thus behavior at t_{rev} is a 'mirror' of the initial motion. Within the hyperpolarizability mechanism, the molecules get an instantaneous kick from the $\delta(t)$ pulse, but the spatial orientation distribution remains unchanged. It takes a short time for the imparted angular momentum to cause the molecules to rotate toward a point of maximum orientation. This is the exact behavior seen in Fig. 6. Within the ionization depletion mechanism, the $\delta(t)$ pulse instantaneously generates non-zero orientation by directly modulating the angular distribution. The instantaneously-generated orientation should then disperse as the molecules start to rotate. Again, this is clearly seen in Fig. 6.

Including now the effects of alignment to the laser-induced orientation results in the revival structures seen in the bottom panel of Fig. 6. The hyperpolarizability revival becomes asymmetric, but does not change position, while the ionization depletion revival keeps its basic shape, but shifts to later times. The coupling of the alignment to the ionization depletion revivals is qualitatively clear. The $\delta(t)$ pulse first creates instantaneous orientation. Then, as the $\cos^2\theta$ interaction generates a torque that squeezes the angular distribution toward molecular alignment, the instantaneously-generated orientation is also squeezed toward greater orientation as the alignment

maximizes (Figs. 4, 5). The coupling between the alignment dynamics and the hyperpolarizability-generated orientation revival is not as obvious, but it is still accounted for by the coupling between the aligning and orienting forces.

Two mechanisms of laser-induced molecular orientation, due to hyperpolarizability and ionization depletion, were studied using the CO molecule as a model system. At low intensities, the hyperpolarizability mechanism dominates the generation of molecular orientation. Once the ionizing intensities are reached, the ionization depletion mechanism dominates. The two orientation mechanisms have clear parallels to the well-known sources of vibrational wave packets: impulsive stimulated Raman scattering (ISRS) [19], and R-dependent ionization ("lochfrass" [20]). Indeed, the hyperpolarizability mechanism acts by imparting angular momentum on the system, similar to ISRS. The ionization depletion on the other hand, directly "burns-in" the rotational wave packet in the coordinate representation, analogously to lochfrass. The orientation revivals contain an unambiguous signature of the active orientation mechanism. the hyperpolarizability mechanism, the peak of the orientation revival precedes the revival time t_{rev}, while for the ionization depletion mechanism the peak of the orientation revival lags behind t_{rev}. These signatures arise due to interplay of the aligning and orienting interactions.

[1] H. Stapelfeldt and T. Seideman, Rev. Mod. Phys. **75**, 543 (2003).

[2] F. Krausz and M. Ivanov, Rev. Mod. Phys. **81**, 163 (2009).

[3] C.Z. Bisgaard, O.J. Clarkin, G. Wu, A.M.D. Lee, O. Geßner, C.C. Hayden, and A. Stolow, Science **323**, 1464 (2009).

[4] S. De, I. Znakovskaya, D. Ray, F. Anis, N. G. Johnson, I. A. Bocharova, M. Magrakvelidze, B. D. Esry, C. L. Cocke, I. V. Litvinyuk, and M. F. Kling, Phys. Rev. Lett. **103**, 153002 (2009);

[5] T. Kanai and H. Sakai, J. Chem. Phys. **115**, 5492 (2001).

[6] B. Friedrich and D. Herschbach, Phys. Rev. Lett. **74**, 4623 (1995).

[7] P.J. Linstrom and W.G. Mallard, Eds., NIST Chemistry WebBook, NIST Standard Reference Database Number 69, National Institute of Standards and Technology, Gaithersburg MD, 20899, http://webbook.nist.gov, (retrieved September 25, 2011).

[8] K. A. Peterson and T. H. Dunning, Jr., J. Mol. Struct. (Theochem) **400**, 93 (1997).

[9] L. D. Landau, E. M. Lifshitz, *Quantum Mechanics: Non-Relativistic Theory*, 3^{rd} edn. (Pergamon, Oxford 1977).

[10] L. V. Keldysh, Zh. Eksp. Teor. Fiz. **47**, 1945 (1964) [English transl.: Sov. Phys. JETP **20**, 1307 (1965)].

[11] M. Spanner and S. Patchkovskii, Chem. Phys. (*in press*, http://dx.doi.org/10.1016/j.chemphys.2011.12.016, 2012).

[12] M. Spanner and S. Patchkovskii, Phys. Rev. A **80**, 063411 (2009).

[13] M.W. Schmidt, K.K. Baldridge, J.A. Boatz, S.T. Elbert, M.S. Gordon, J.H. Jensen, S. Koseki, N. Matsunaga, K.A. Nguyen, S. Su, T.L. Windus, M. Dupuis, and J.A. Montgomery, J. Comput. Chem. **14**, 1347 (1993).

[14] T.H. Dunning, Jr., Chem. Phys. **90**, 1007 (1989).

[15] D.E. Manolopoulos, J. Chem. Phys. **117**, 9552 (2002).

[16] W. H. Press, B. P. Flannery, S. A. Teukolsky, and W. T. Vetterling, *Numerical Recipes*, Cambridge University Press, Cambridge, 2^{nd} edition, 1992.

[17] E. Frumker, C.T. Hebeisen, N. Kajumba, J.B. Bertrand, H.J. Wörner, M. Spanner, D.M. Villeneuve, A. Naumov, and P. B. Corkum (*in submitted*, 2012).

[18] This model accurately captures the temporal dynamics of the orientation, but no longer includes the decay of the total wavefunction amplitude caused by ionization. The population decay can be recovered by restoring the θ-independent omponent of $V_I'(\theta)$ in Eq. (15).

[19] S. de Silvestri, J.G. Fujimoto, E.P. Ippen, E.B. Gamble Jr., L.R. Williams, and K.A. Nelson, Chem. Phys. Lett. **116**, 146 (1985).

[20] E. Goll, G. Wunner, and A. Saenz, Phys. Rev. Lett. **97**, 103003 (2006).